RSC Advances

PAPER

View Article Online
View Journal | View Issue

Open Access Article. Published on 26 July 2017. Downloaded on 11/21/2025 10:08:16 PM.
This article is licensed under a Creative Commons Attribution-NonCommercial 3.0 Unported Licence.

Check for updates

Cite this: *RSC Adv.*, 2017, 7, 36917

Phase transformations of vanadium recovery from refractory stone coal by novel NaOH molten roasting and water leaching technology

Zhenlei Cai *abc and Yimin Zhang *abcd

Received 27th April 2017
Accepted 10th July 2017

DOI: 10.1039/c7ra04741j

rsc.li/rsc-advances

In this study, a novel NaOH molten roasting and water leaching technology, an eco-friendly process with good selectivity and good availability, was investigated for vanadium recovery from refractory stone coal. In addition, the phase transformations during the vanadium recovery process were also studied. During the NaOH molten roasting process, the monoclinic crystalline structure of muscovite ($K(Al,V)_2[Si_3AlO_{10}](OH)_2$) was converted into the orthorhombic crystalline structure of Na_2SiO_3 and the tetragonal crystalline structure of gehlenite ($Ca_2Al_2SiO_7$); this could promote the liberation and recovery of vanadium. During the water leaching process, the tetragonal crystalline structure of gehlenite ($Ca_2Al_2SiO_7$) was converted into the monoclinic crystalline structure of $Ca_3Si_2O_7 \cdot H_2O$. $Ca_3Si_2O_7 \cdot H_2O$, a kind of C–S–H gel, produced during the water leaching process probably covered the surface of the roscoelite and thus prevented effective vanadium recovery from roscoelite.

1. Introduction

Vanadium plays significant roles in many fields such as ferrous and nonferrous alloy production,[1] catalysts,[2] and redox flow batteries.[3] More than 87% of the vanadium resources exist as stone coal in China. Moreover, most of them are refractory for vanadium recovery because vanadium in this stone coal usually exists as isomorphism substitution in the mica (muscovite or illite) lattice structure, which is named as roscoelite.[4]

In recent years, many additives were employed for the recovery of vanadium from different vanadium resources, which could be divided into leaching additives and roasting additives. The study on the leaching additives utilized for vanadium slag or spent catalysts was mainly focused on oxalic acid,[5] $NaClO_3$,[6] Na_2SO_3,[7] *etc.* Moreover, the existence of leaching additives for vanadium recovery from stone coal is universal. These additives primarily include $FeSO_4$,[8] NaClO,[9] CaF_2,[10] H_2SiF_6,[11] *etc.* Most of these leaching additives are effectively used under acidic conditions, resulting in lower selectivity and increased dissolution of impurities. The increase in impurity concentration probably causes negative effects in the subsequent purification process. Although there have been a few investigations on the basic additives for the vanadium recovery from stone coal, such as on the use of NaOH[12] solution for vanadium leaching from roasted stone coal, the efficiency of vanadium recovery is low since high roasting or leaching temperature and extended roasting time are required.

Based on the developments of the roasting additives and technologies for the vanadium recovery, Na_2CO_3 (ref. 13 and 14) and CaO[15] were effective roasting additives. They were not, however, suitable for vanadium recovery from stone coal with high alumino–silicate content because of the requirement for high roasting temperatures. Although the utilization of NaCl[16] or Na_2SO_4 (ref. 17) was relatively effective for vanadium extraction from stone coal, it was gradually restricted in China because of serious poisonous emissions of Cl_2, HCl or SO_2 gases. The effect of calcified roasting *via* $CaCO_3$ (ref. 18) or $Ca(OH)_2$ (ref. 19) on vanadium extraction from stone coal was limited because of low crystalline destruction of roscoelite and vanadium oxidation degree. Moreover, composite additives such as NaCl and CaO can also be effective for vanadium extraction from stone coal and remove Cl from fuel gas, but their application has been confined to a fluidized bed roasting reactor.[20] Recently, our research group reported a novel $BaCO_3$/CaO composite roasting additive and acid leaching technology for vanadium recovery from stone coal. However, its industrial application and feasibility remains to be further studied.[21,22]

While the NaOH molten roasting technology exhibits eco-friendliness (no discharge of poisonous gases and wastes), good selectivity (low extraction of impurities), and good availability (low roasting temperature and high recovery efficiency), to date, it has only been applied for the recovery of titanium or chromium from secondary resources.[23,24] However, the

[a]School of Resource and Environmental Engineering, Wuhan University of Science and Technology, Wuhan 430081, China. E-mail: caizhenlei@wust.edu.cn; ande559@163.com; zym126135@126.com

[b]Hubei Provincial Engineering Technology Research Center of High Efficient Cleaning Utilization for Shale Vanadium Resource, Wuhan 430081, China

[c]Hubei Collaborative Innovation Center for High Efficient Utilization of Vanadium Resources, Wuhan 430081, China

[d]School of Resource and Environmental Engineering, Wuhan University of Technology, Wuhan 430070, China

Open Access Article. Published on 26 July 2017. Downloaded on 11/21/2025 10:08:16 PM.
This article is licensed under a Creative Commons Attribution-NonCommercial 3.0 Unported Licence.

feasibility and applicability of this technology to vanadium recovery from stone coal, especially for high alumino–silicate-containing refractory stone coal, still lacks sufficient scientific evidence. In addition, the phase transformation and the ion leaching behavior during the recovery process require further investigation for the guidance and reference of this technology.

In this study, the effectiveness of the novel NaOH molten roasting and water leaching technology for vanadium recovery from refractory stone coal was investigated. Many technical conditions were optimized, and the leaching behaviors of vanadium, silicon, aluminum, and potassium were studied. Moreover, the phase transformations were also investigated to reveal the mechanisms responsible for the vanadium recovery process.

2. Materials and methods

2.1. Materials

The raw stone coal was obtained from Hubei, China. The raw ore was crushed and ground into powder with the particle size of −0.074 mm accounting for 75% of the sample. The chemical multi-elemental analysis of the raw stone coal is listed in Table 1. The main mineral phase compositions of the raw stone coal, which were determined by XRD (Fig. 1), included quartz, muscovite, phlogopite, calcite, and pyrite. The electron microprobe analysis of the raw stone coal is provided in Table 2. The vanadium-containing minerals mainly consisted of muscovite and illite.

The raw stone coal was subjected to carbon removal pretreatment by blank roasting in a muffle furnace at 750 °C for 1 h. The chemical multi-elemental analysis and the XRD pattern of the blank roasted sample are shown in Table 1 and Fig. 1, respectively. The results when compared with those of the raw ore indicated that the V_2O_5 content increased to 0.91% and the crystalline phase diffraction peak of pyrite was converted into that of hematite. Additionally, a new crystalline phase diffraction peak of anhydrite appeared. The BEI and EDS elemental distributions of the blank roasted sample are shown in Fig. 2. The EDS spectra analysis of the (i) point showed that the aluminium content was 11.80%, which was close to the theoretical aluminium content 12.80% of muscovite ($(K(Al,V)_2[Si_3AlO_{10}](OH)_2)$) containing vanadium. Moreover, the relevance of V, O, Al, Si, and K in the blank roasted sample indicated that vanadium probably existed in muscovite ($(K(Al,V)_2[Si_3AlO_{10}](OH)_2)$).

2.2. Experimental procedure

Herein, 20 g of blank roasted sample was added to a nickel crucible with a certain mass ratio of NaOH added to it and completely mixed. After the crucible was placed in a muffle furnace, the NaOH molten roasting process was started at the required temperature for a certain period of time. When the roasting process was complete, the roasted product was transferred to a leaching pod containing 100 mL water. The solution was continuously stirred at the required temperature for a certain period. After the leaching solution was filtrated, vanadium, silicon, aluminium, and potassium in the filtrate were analysed by ICP-OES to calculate the leaching efficiency. The leaching efficiency can be calculated as follows:

$$\eta = \frac{V\beta}{m\alpha} \times 100\% \quad (1)$$

where η is the leaching efficiency for a certain element (wt%), V is the volume of the filtrate (mL), β is the content for a certain element in filtrate (g mL^{-1}), m is the mass of the blank roasted sample of stone coal (g), and α is the content for a certain element in the blank roasted sample of stone coal (wt%).

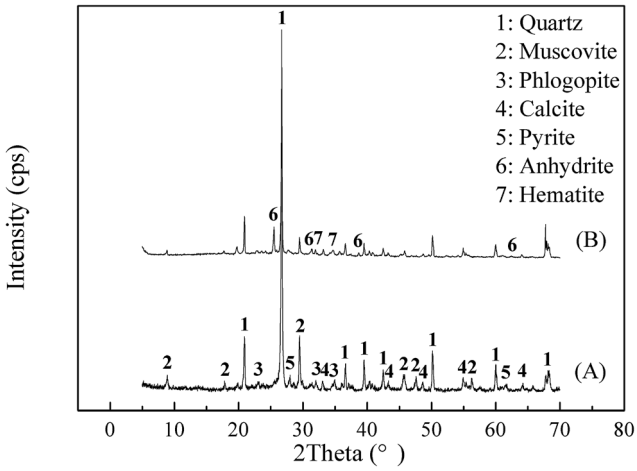

Fig. 1 XRD image of raw stone coal and blank roasted sample. ((A) Raw stone coal, (B) blank roasted sample).

Table 2 Electron microprobe analysis of raw stone coal (wt%)

Mineral	SiO_2	V_2O_3	Al_2O_3	FeO	MgO	CaO	Na_2O	K_2O
Pyrite	0.06	0.00	0.00	59.12	0.00	0.00	0.00	0.00
Calcite	0.03	0.00	0.00	0.07	0.55	63.44	0.00	0.00
Quartz	98.35	0.00	0.00	0.00	0.00	0.00	0.00	0.00
Muscovite	51.08	3.48	27.22	0.23	4.53	0.02	0.07	9.52
Illite	31.88	2.25	16.98	0.18	1.56	0.74	0.02	6.11
Anorthose	56.94	0.00	25.25	0.00	0.10	6.51	6.82	0.98

Table 1 Chemical multi-elemental analysis of raw stone coal and blank roasted sample (wt%)

	V_2O_5	SiO_2	Al_2O_3	CaO	Fe_2O_3	K_2O	MgO	Na_2O	SO_3	P_2O_5	TC
Raw stone coal	0.77	51.15	9.08	8.33	2.44	1.97	1.82	0.45	3.55	1.29	17.89
Blank roasted sample	0.91	56.36	10.69	9.27	2.83	3.81	2.75	0.44	1.42	1.18	2.67

 This journal is © The Royal Society of Chemistry 2017

Open Access Article. Published on 26 July 2017. Downloaded on 11/21/2025 10:08:16 PM.
This article is licensed under a Creative Commons Attribution-NonCommercial 3.0 Unported Licence.

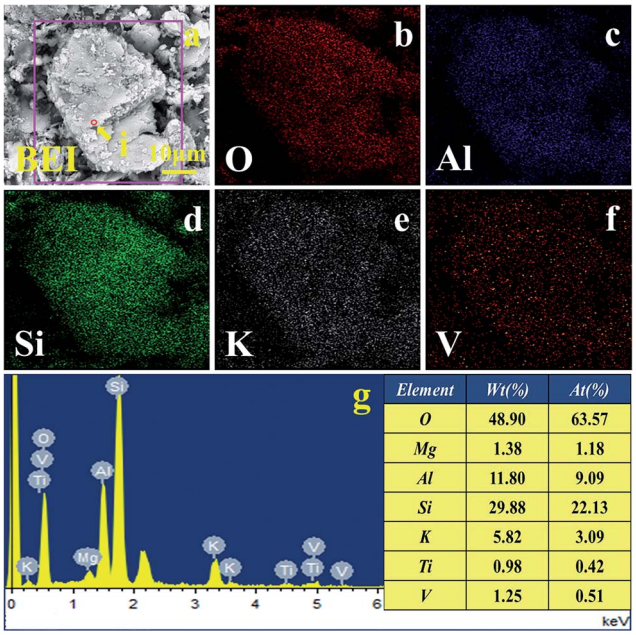

Element	Wt(%)	At(%)
O	48.90	63.57
Mg	1.38	1.18
Al	11.80	9.09
Si	29.88	22.13
K	5.82	3.09
Ti	0.98	0.42
V	1.25	0.51

Fig. 2 (a) BEI of blank roasted sample, EDS elemental distribution: (b) O; (c) Al; (d) Si; (e) K; (f) V and (g) EDS spectra marked from BEI by circle.

3. Results and discussion

3.1. NaOH molten roasting process

3.1.1. Effects of mass ratio of NaOH to blank roasted sample and roasting time on vanadium leaching efficiency. The effects of mass ratio of NaOH to blank roasted sample and roasting time on the vanadium leaching efficiency are shown in Fig. 3, and the roasting temperature is fixed at 550 °C. The vanadium leaching efficiency increased with the increasing mass ratio of NaOH to blank roasted sample until the mass ratio was 1 : 1, when the condition of the roasting temperature was intermediate level (550 °C). The vanadium leaching efficiency increased with the extension of the roasting time. When the roasting time was 1.5 h, the vanadium leaching efficiency was maximized.

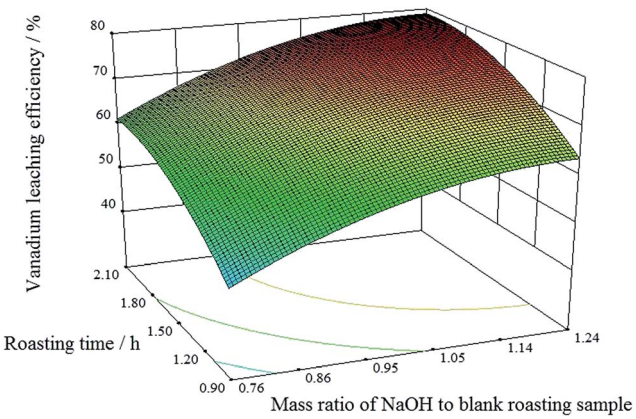

Fig. 3 Effects of mass ratio of NaOH to blank roasted sample and roasting time on vanadium leaching efficiency.

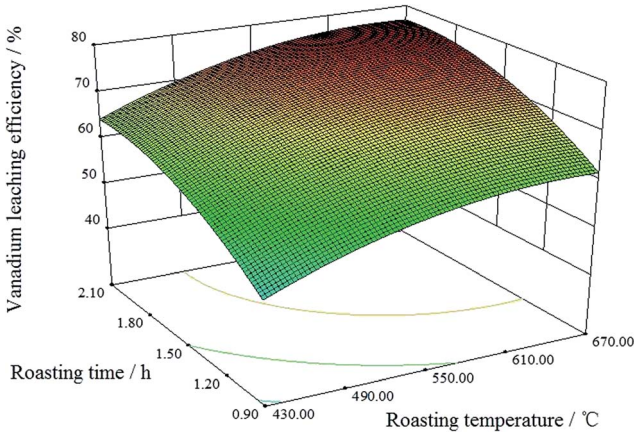

Fig. 4 Effects of roasting temperature and roasting time on vanadium leaching efficiency.

3.1.2. Effects of roasting temperature and roasting time on vanadium leaching efficiency. Effects of roasting temperature and roasting time on vanadium leaching efficiency are presented in Fig. 4, with a fixed mass ratio of NaOH to blank roasted sample at 1 : 1. The vanadium leaching efficiency did not reduce until the roasting temperature was over 550 °C when the condition of the mass ratio was intermediate level (1 : 1). Longer roasting times benefited the vanadium leaching efficiency. However, when the roasting time was over 1.5 h, further extension of the roasting time only slightly improved the vanadium leaching efficiency.

3.1.3. Phase transformation during the NaOH molten roasting process. The phase transformation of the samples during roasting was studied using XRD; a mass ratio of NaOH to blank roasted sample of 1 : 1 and a roasting temperature of 550 °C were used, with the roasting time ranging from 10 min to 90 min. The XRD patterns are shown in Fig. 5. The results indicated that the muscovite and phlogopite crystalline phases disappeared, and new crystalline phases of Na_2SiO_3 and gehlenite were present in the roasted sample, indicating that the

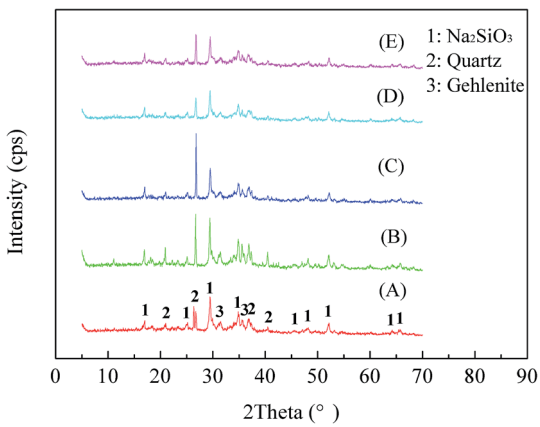

Fig. 5 XRD patterns of roasted samples at different roasting times. ((A) roasting for 10 min; (B) roasting for 20 min; (C) roasting for 30 min; (D) roasting for 60 min (E) roasting for 90 min).

Open Access Article. Published on 26 July 2017. Downloaded on 11/21/2025 10:08:16 PM.
This article is licensed under a Creative Commons Attribution-NonCommercial 3.0 Unported Licence.

structure of muscovite or phlogopite was effectively destroyed. The diffraction peaks of the quartz crystalline phase were first enhanced during the first 30 min of roasting and then weakened in the following period. This is mainly because of the selective dissolution of mica during the NaOH molten roasting process in the first period and the dissolution of quartz in the subsequent stage. Moreover, V(III), which was an isomorphic replacement of Al(III) in the octahedral alumina in the mica of stone coal, was liberated from the crystal lattice and oxidized into V(IV) or V(V) for the preparation of the following water leaching process.

The crystal transformation relationship of muscovite ($K(Al,V)_2[Si_3AlO_{10}](OH)_2$), Na_2SiO_3, and gehlenite ($Ca_2Al_2SiO_7$) is shown in Fig. 6. The crystalline structure of muscovite ($K(Al,V)_2[Si_3AlO_{10}](OH)_2$) is with a monoclinic crystal system, and the unit cell parameters are $a = 0.5193$ nm, $b = 0.9045$ nm, $c = 2.0044$ nm, $\alpha = \gamma = 90°$, and $\beta = 95.8°$. During the NaOH molten roasting process, Si–O and Al–O bonds were broken. Moreover, the orthorhombic structure of Na_2SiO_3 and the tetragonal structure of gehlenite ($Ca_2Al_2SiO_7$) were formed. The crystalline structure of Na_2SiO_3 is with the $CMC2_1$ space group and the unit cell parameters are $a = 1.0466$ nm, $b = 0.603$ nm, $c = 0.471$ nm, and $\alpha = \beta = \gamma = 90°$. The crystalline structure of gehlenite ($Ca_2Al_2SiO_7$) is with the $P\bar{4}21m$ space group and the unit cell parameters are $a = b = 0.7693$ nm, $c = 0.5072$ nm, and $\alpha = \beta = \gamma = 90°$. Al^{3+} ion and the Si^{4+} ion locate at the same position in the unit cell with different occupancies. Al–Si–O oxides form a double close packed type array with the inclusion of Ca^{2+} through tetragonal coordination.

The crystal transformation usually includes two steps: modification and reconstruction. The modification only refers to the change of cell parameters, but not the chemical bonds. However, reconstruction refers to the original large area breakage of chemical bonds and the rebuilding of new structure. Therefore, according to the abovementioned analysis, the phase transformation in the NaOH molten roasting process belongs to the reconstruction, and vanadium can be liberated during this process. The reaction equation corresponding to the phase transformation in the NaOH molten roasting process is as follows:

$$\begin{aligned} &2K(Al,V)_2[Si_3AlO_{10}](OH)_2\ \text{(muscovite)} \\ &\qquad + 6NaOH + 6CaCO_3 + 5O_2 \rightarrow \\ &3Na_2SiO_3 + 3Ca_2Al_2SiO_7\ \text{(gehlenite)} \\ &\qquad + 2V_2O_5 + K_2O + 6CO_2 + 5H_2O \end{aligned} \tag{2}$$

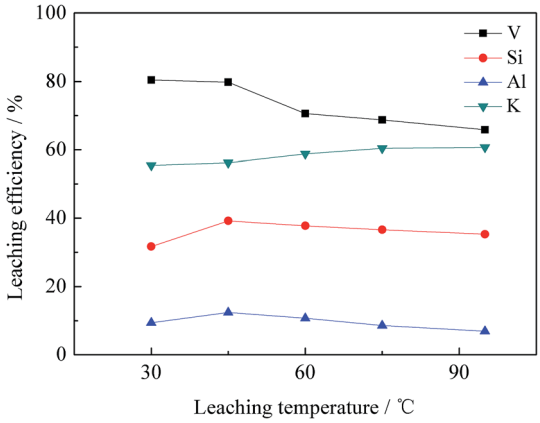

Fig. 7 Effect of leaching temperature on leaching efficiency of vanadium, silicon, aluminium and potassium.

3.2. Water leaching process

3.2.1. Effect of leaching temperature. The effect of leaching temperature from 30 °C to 95 °C on the leaching efficiency of vanadium, silicon, aluminium, and potassium is shown in Fig. 7, with a leaching time of 2 h and a liquid-to-solid ratio of 5 mL g^{-1}. It can be seen that the vanadium leaching efficiency gradually decreased with the leaching temperature ranging from 30 °C to 95 °C. Moreover, the leaching efficiency of silicon and aluminium increased until 45 °C and then decreased with increasing leaching temperature. This is mainly because of the production and dissolution of sodium aluminate and sodium silicate in the initial period. However, with the increase of leaching temperature, the reaction activity was enhanced and the sodium alumino–silicate precipitated, which could therefore result in the adsorption and inclusion loss of vanadium.[25,26] The potassium leaching efficiency slightly increased with increasing leaching temperature. Therefore, the optimum leaching temperature should be 30 °C.

3.2.2. Effect of leaching time. The effect of leaching time in the range from 10 min to 180 min on the leaching efficiency of vanadium, silicon, aluminium, and potassium is shown in Fig. 8, with a fixed leaching temperature of 550 °C and a liquid-to-solid ratio of 5 mL g^{-1}. The results indicated that the potassium leaching efficiency steadily increased with the increasing leaching time. In contrast, the similar change

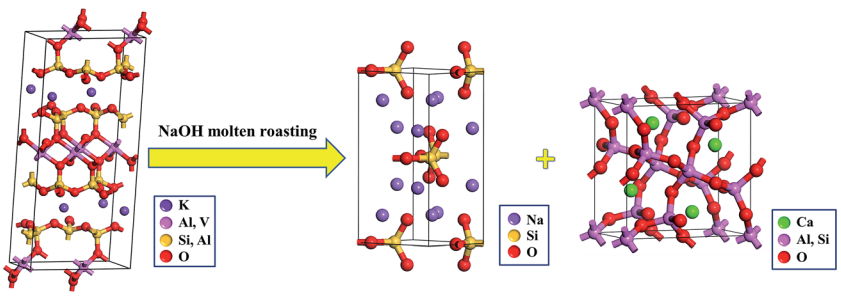

Fig. 6 Crystal transformation relationship of muscovite ($K(Al,V)_2[Si_3AlO_{10}](OH)_2$), Na_2SiO_3 and gehlenite ($Ca_2Al_2SiO_7$) in the NaOH molten roasting process.

Open Access Article. Published on 26 July 2017. Downloaded on 11/21/2025 10:08:16 PM.
This article is licensed under a Creative Commons Attribution-NonCommercial 3.0 Unported Licence.

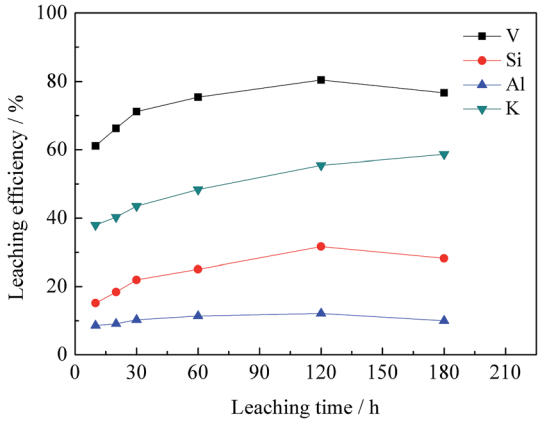

Fig. 8 Effect of leaching time on leaching efficiency of vanadium, silicon, aluminium and potassium.

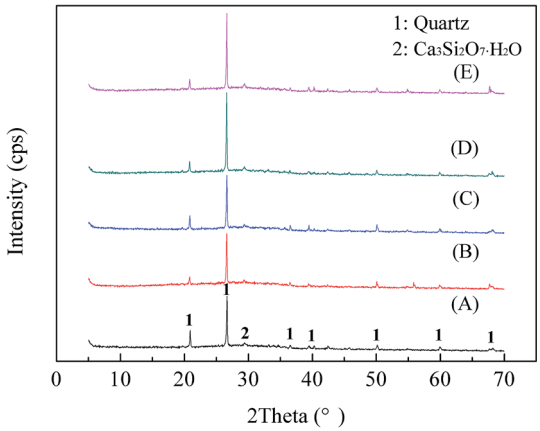

Fig. 9 XRD patterns of water leaching residuals at different leaching times. ((A) leaching for 10 min; (B) leaching for 20 min; (C) leaching for 30 min; (D) leaching for 60 min; (E) leaching for 120 min).

tendency of the leaching efficiency of vanadium, silicon, and aluminium during the water leaching process could be obtained, *i.e.* it increased in the initial period of 120 min and then decreased till 180 min. The leaching efficiency of vanadium, silicon, aluminium, and potassium was 80.44%, 31.66%, 12.14%, and 55.45%, respectively. Therefore, the optimum leaching time should be 120 min.

The chemical multi-elemental analysis of the leachate under the optimal conditions is shown in Table 3. The V_2O_5 content was 0.72 g L^{-1}, and the main impurities were SiO_2 (22.54 g L^{-1}), K_2O (2.28 g L^{-1}), and Al_2O_3 (1.28 g L^{-1}).

3.2.3. Phase transformation during the water leaching process. The phase transformation during the water leaching process was investigated according to the XRD analysis of the leaching residuals from 10 min to 120 min, with a fixed leaching temperature of 550 °C and a liquid-to-solid ratio of 5 mL g^{-1}. The XRD patterns are shown in Fig. 9. The results indicated that the Na_2SiO_3 and gehlenite crystalline phases in the NaOH roasting samples disappeared, whereas the diffraction peaks of the quartz crystalline phase in the water leaching residuals intensified with the increasing leaching time from 10 min to 120 min. In addition, the new crystalline phase of $Ca_3Si_2O_7 \cdot H_2O$ formed in the water leaching residuals.

The crystal transformation relationship of gehlenite ($Ca_2Al_2SiO_7$) and $Ca_3Si_2O_7 \cdot H_2O$ is shown in Fig. 10. During the water leaching process, the Al–O bond of gehlenite ($Ca_2Al_2SiO_7$) was broken. Moreover, the Ca–Si and Ca–O bonds were shaped, and the monoclinic structure of $Ca_3Si_2O_7 \cdot H_2O$ was formed. The crystalline structure of $Ca_3Si_2O_7 \cdot H_2O$ is with the $P2_1/M$ space group and the unit cell parameters are $a = 0.6824$ nm, $b = 1.5465$ nm, $c = 0.6839$ nm, $\alpha = \gamma = 90°$, and $\beta = 97.692°$. The reaction equation corresponding to the phase transformation during the water leaching process is as follows:

Table 3 Chemical multi-elemental analysis of leachate (g L^{-1})

Element	V_2O_5	SiO_2	K_2O	Al_2O_3	CaO	MgO
Content	0.72	22.54	2.28	1.28	0.50	0.08

$$3Ca_2Al_2SiO_7 \text{ (gehlenite)} + Na_2SiO_3 + 4NaOH \rightarrow 2Ca_3Si_2O_7 \cdot H_2O + 6NaAlO_2 \quad (3)$$

The BEI and EDS elemental distributions of water leaching residual are shown in Fig. 11. The results indicate that the

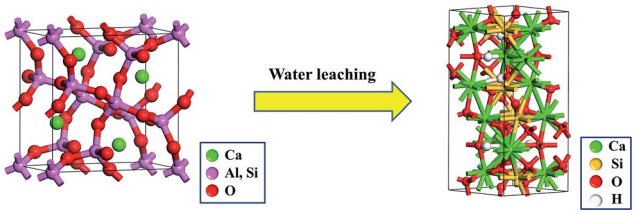

Fig. 10 Crystal transformation relationship of gehlenite ($Ca_2Al_2SiO_7$) and $Ca_3Si_2O_7 \cdot H_2O$ in the water leaching process.

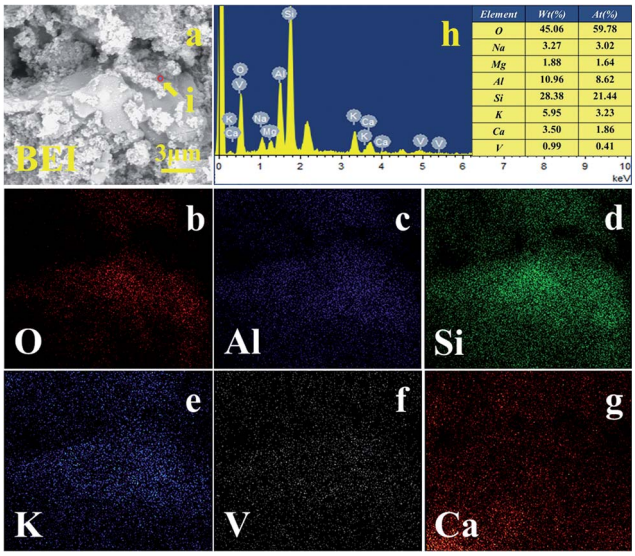

Fig. 11 (a) BEI of water leaching residual, EDS elemental distribution: (b) O; (c) Al; (d) Si; (e) K; (f) V; (g) Ca and (h) EDS spectra marked from BEI by circle.

Open Access Article. Published on 26 July 2017. Downloaded on 11/21/2025 10:08:16 PM.
This article is licensed under a Creative Commons Attribution-NonCommercial 3.0 Unported Licence.

element distribution of O, Si, and Ca have obvious relevance. Combined with the XRD analysis of the water leaching residual, $Ca_3Si_2O_7 \cdot H_2O$ indeed existed after the NaOH molten roasting and water leaching process. The EDS spectra analysis of the (i) point showed that the aluminium content was 10.96%, which was close to the theoretical aluminium content 12.80% of muscovite ($K(Al,V)_2[Si_3AlO_{10}](OH)_2$) containing vanadium. Moreover, the relevance of V, O, Al, Si, and K in the leaching residual indicated that there was still a small amount of roscoelite left in the leaching residual. $Ca_3Si_2O_7 \cdot H_2O$, a kind of C–S–H gel,[27] produced during the water leaching process probably covered the surface of the roscoelite and thus prevented the effective recovery of vanadium from the roscoelite.

4. Conclusions

(1) The novel NaOH molten roasting and water leaching technology, an eco-friendly process with good selectivity and good availability, was found to be feasible for the recovery of vanadium from refractory stone coal.

(2) During the NaOH molten roasting process, the monoclinic crystalline structure of muscovite ($K(Al,V)_2[Si_3AlO_{10}](OH)_2$) in stone coal was converted into the orthorhombic crystalline structure of Na_2SiO_3 and the tetragonal crystalline structure of gehlenite ($Ca_2Al_2SiO_7$), which could promote the liberation and recovery of vanadium.

(3) During the water leaching process, the tetragonal crystalline structure of gehlenite ($Ca_2Al_2SiO_7$) was converted into the monoclinic crystalline structure of $Ca_3Si_2O_7 \cdot H_2O$. $Ca_3Si_2O_7 \cdot H_2O$, a kind of C–S–H gel, produced during the water leaching process probably covered the surface of the roscoelite and thus prevented the effective recovery of vanadium from the roscoelite.

Acknowledgements

This work was financially supported by the National Natural Science Foundation of China (No. 51604197) and the Natural Science Foundation of Hubei Province, China (No. 2016CFB197).

References

1 W. Li, Y. M. Zhang, T. Liu, J. Huang and Y. Wang, *Hydrometallurgy*, 2013, **131**, 1.
2 Y. T. Chen, W. Chen, Q. H. Tang, Z. Guo, Y. H. Yang and F. B. Su, *Catal. Lett.*, 2011, **141**, 149.
3 T. Hong and F. Q. Xue, *Paper presented at the 2009 Asia-Pacific Power and Energy Engineering Conference*, 2009, p. 1.
4 X. B. Li, C. Wei, Z. G. Deng, M. T. Li, C. X. Li and G. Fan, *Hydrometallurgy*, 2011, **105**, 359.
5 K. Mazurek, *Hydrometallurgy*, 2013, **134–135**, 26.
6 K. Yang, X. Zhang, X. Tian, Y. Yang and Y. Chen, *Hydrometallurgy*, 2010, **103**, 7.
7 M. D. Okudan, A. Akcil, A. Tuncuk and H. Deveci, *Hydrometallurgy*, 2015, **152**, 76.
8 M. T. Li, C. Wei, G. Fan, C. X. Li, Z. G. Deng and X. B. Li, *Trans. Nonferrous Met. Soc. China*, 2010, **20**, s112.
9 C. X. Li, C. Wei, Z. G. Deng, M. T. Li, X. B. Li and G. Fan, *Trans. Nonferrous Met. Soc. China*, 2010, **20**, s127.
10 Z. J. Ju, C. Y. Wang and F. Yin, *Int. J. Miner. Process.*, 2015, **138**, 1.
11 X. Zhang, K. Yang, X. Tian and W. Qin, *Int. J. Miner. Process.*, 2011, **100**, 184.
12 D. He, Q. Feng, G. Zhang, L. Ou and Y. Lu, *Miner. Eng.*, 2007, **20**, 1184.
13 M. Aarabi-Karasgani, F. Rashchi, N. Mostoufi and E. Vahidi, *Hydrometallurgy*, 2010, **102**, 14.
14 H. Y. Li, H. X. Fang, K. Wang, W. Zhou, Z. Yang, X. M. Yan, W. S. Ge, Q. W. Li and B. Xie, *Hydrometallurgy*, 2015, **156**, 124.
15 W. C. Song, H. Li, F. X. Zhu, K. Li and Q. Zheng, *Trans. Nonferrous Met. Soc. China*, 2014, **24**, 2687.
16 M. Wang, X. Xiang, L. Zhang and L. Xiao, *Rare Met.*, 2008, **27**, 112.
17 Y. Zhao, Y. Zhang, S. Bao, T. Chen and X. Liu, *Ind. Eng. Chem. Res.*, 2014, **53**, 157.
18 C. L. Li, X. Y. Zhou, H. Wang, T. K. Zhang, J. Li, X. Ou and X. D. Jiang, *J. Cent. South Univ.*, 2011, **42**, 7.
19 G. Zhang and S. Ma, *Chin. J. Rare Met.*, 2007, **31**, 813.
20 X. Zeng, F. Wang, H. Zhang, L. Cui, J. Yu and G. Xu, *Fuel*, 2015, **142**, 180.
21 Z. L. Cai, Y. M. Zhang, T. Liu and J. Huang, *Minerals*, 2016, **6**, 14.
22 Z. L. Cai, Y. M. Zhang, T. Liu and J. Huang, *JOM*, 2015, **67**, 2629.
23 Z. H. Wang, S. L. Zheng, S. N. Wang, B. Liu, D. W. Wang, H. Du and Y. Zhang, *Trans. Nonferrous Met. Soc. China*, 2014, **24**, 1273.
24 D. S. Chen, L. S. Zhao, Y. H. Liu, T. Qi, J. C. Wang and L. N. Wang, *J. Hazard. Mater.*, 2013, **244–245**, 588.
25 E. B. Webb and S. H. Garofalini, *Surf. Sci.*, 1994, **319**, 381.
26 W. E. Adam, K. Neumann and J. P. Ploumen, *Fette, Seifen, Anstrichm.*, 1979, **81**, 445.
27 O. Mendoza, C. Giraldo, S. S. Camargo Jr and J. I. Tobón, *Cem. Concr. Res.*, 2015, **74**, 88.

 This journal is © The Royal Society of Chemistry 2017